MapZ forms a stable ring structure that acts as a track for FtsZ treadmilling in *Streptococcus mutans*

Yongliang Li[1], Shipeng Shao[2], Xiao Xu[1], Xiaodong Su[3], Yujie Sun[2*], Shicheng Wei[1*]

1. Central Laboratory/Department of Oral and Maxillofacial Surgery, School and Hospital of Stomatology, Peking University; National Engineering Laboratory for Digital and Material Technology of Stomatology, Beijing 100081, China

2. State Key Laboratory of Membrane Biology, Biodynamic Optical Imaging Center (BIOPIC), School of Life Sciences, Peking University, Beijing 100871, China

3. State Key Laboratory of Protein and Plant Gene Research, School of Life Sciences, Peking University, Beijing 100871, China.

*: Correspondence: Shicheng Wei[1] or Yujie Sun[2]

1. Central Laboratory/Department of Oral and Maxillofacial Surgery, School and Hospital of Stomatology, Peking University, 22 Zhonguancun South Road, Haidian District, Beijing 100081, China Tel: (+86)-10-82195771; E-mail address: sc-wei@pku.edu.cn

2. State Key Laboratory of Membrane Biology, Biodynamic Optical Imaging Center (BIOPIC), School of Life Sciences, Peking University, 5 Yiheyuan Road Beijing 100871, China Tel: (+86)-10-62744060; E-mail address: sun_yujie@pku.edu.cn

Abstract

Proper formation of the FtsZ ring at the site of division is crucial for initiation of bacterial cell division. A number of systems have been reported to regulate the spatial localisation of the FtsZ ring. MapZ, a recently identified FtsZ regulatory protein in *Streptococcaceae*, has been found to mark the division site and position the FtsZ ring. However, it is unclear how MapZ regulates the dynamics of the FtsZ ring in *Streptococcaceae*, which is important for understanding the underlying mechanism of this system. Here, we studied how MapZ regulates the FtsZ ring in *Streptococcus mutans*, and its effect on the directional motion of FtsZ filaments. The results show that FtsZ filaments in the ring exhibited treadmilling motion in *S. mutans*, similar to that in *Escherichia coli* and *Bacillus subtilis*. Interestingly, deletion of MapZ led to unconstrained movement of treadmilling FtsZ filaments and a shorter lifetime of the constricting FtsZ ring. Furthermore, using both super resolution imaging and single molecule tracking, we revealed that MapZ forms an immobile ring-like structure at the division site. Taken together, this study suggests that MapZ forms a stable ring that acts as a track for FtsZ treadmilling in *S. mutans*.

In bacteria, the tubulin homologue FtsZ is a core component of the division machinery. On the initiation of cell division, FtsZ forms a ring structure called the Z ring, which localises to the middle of a cell[1] and recruits other components to construct the division machinery[2]. Over the past few decades, a number of studies have focused on the Z-ring as well as its regulatory system. The Min system[3], which includes three proteins, MinC, MinD, and MinE, was the first division site selection system discovered in *Escherichia coli*. Oscillation of the MinCD complex from pole to pole defines a minimum concentration of MinC at the middle of the cell, which directly prevents FtsZ polymerisation. The nucleoid occlusion (NO) system[4] was also identified, which contains the special DNA-binding proteins SimA and Noc in *E.coli* and *Bacillus subtilis*, respectively. Although

52 both of these proteins have been found to inhibit FtsZ assembly via binding to DNA of the
53 undivided chromosome, a recent study has demonstrated that in addition to these two systems,
54 some other unidentified mechanisms should also play a role in the early stage of cell division in *B.*
55 *subtilis*[5]. However, many bacteria actually lack both of Min and NO systems and they evolved other
56 Z ring regulatory systems. For instance, MipZ[6] was discovered in *Caulobacter crescentus* and is
57 conserved among *α proteobacteria.* It directly perturbs FtsZ polymerisation and forms a complex
58 with the DNA-binding protein ParB, which binds to replication origin regions. The complex
59 restricts FtsZ assembly forming a Z ring in the mid-cell, where MipZ has the lowest concentration.
60 Distinct from the negative regulatory systems mentioned above, two positive control systems
61 PomZ[7] and SsgA/SsgB[8] were identified in *Myxococcus xanthus* and *Streptomyces*, respectively.
62 These two systems localise at the division site prior to FtsZ and directly recruit FtsZ to the mid-cell
63 to form the Z ring.

64 Recently, another important positive regulatory system was discovered in *Streptococcus*
65 *pneumoniae* and is conserved in *Streptococcaceae*, which lack the aforementioned FtsZ regulatory
66 systems. The new system is mediated by the membrane protein MapZ (also called LocZ)[9, 10], which
67 positions the Z ring at the division site and controls its constriction.

68 The extracellular domain of MapZ is composed of two sub-domains,[11] and the subdomain
69 tandem to the transmembrane domain acts as pedestal for proper localisation of the C-terminal
70 domain, which directly binds to peptidoglycan. This two-domain structure implies that the
71 "pedestal" domain may play the role of a switch, thereby regulating the interaction of MapZ and
72 nascent peptidoglycans. This study supports the view that MapZ binds to nascent peptidoglycans
73 at the site of division and is then pushed toward the daughter cell equator by peptidoglycan
74 elongation, thereby marked the future division site. However, a recent study claimed that MapZ is
75 not the initial factor that determines the division site[12]. This study showed that the origin of
76 chromosome replication (oriC), which is located at the site of division prior to the MapZ ring, is

77 crucial for cell division. Deletion of MapZ had no remarkable effect on oriC localisation. However,
78 perturbing the segregation of oriC led to mislocalisation of MapZ.

79 Although it has been shown that MapZ interacts with FtsZ to position the Z-ring, how MapZ
80 regulates the dynamics of the FtsZ ring is unclear. Here, we studied how MapZ regulates the
81 position and movement of the FtsZ ring. The results show that FtsZ filaments in the ring exhibit a
82 treadmilling motion in *Streptococcus mutans*, similar to that in *E. coli* and *B. subtilis*[13, 14]. Deletion
83 of MapZ showed an interesting impact on the movement of treadmilling FtsZ filaments, the plane
84 angle of the FtsZ ring at its early formation stage, and the lifetime of the constricting FtsZ ring.
85 Further, our data revealed a stable ring like structure of MapZ at the division site, suggesting that
86 MapZ ring serves as a track for treadmilling FtsZ filaments in *S. mutans*.

87

88 **Results**

89 **Characterise MapZ homologue in *Streptococcus mutans*.**

90 MapZ was identified in *S. pneumoniae* (spMapZ). Here, we identified a MapZ homologue in
91 *S. mutans* (smMapZ); consistent with a previous report[15], smMapZ shows 37% sequence identity
92 with spMapZ, with 32% and 50% sequence identity for the cytoplasmic and extracellular domains,
93 respectively. Strikingly, most of the first 40 amino acids of spMapZ, which were thought to be
94 sufficient for the interaction of MapZ and FtsZ, were deficient in smMapZ while the two
95 phosphorylation sites[9] (T67 and T78) and the amino acids[11] (R409, Y411, N428, Y430, Y450, F451
96 and N454) required for binding to pneumococcal peptidoglycans are conserved (Extended Data 1a).
97 Subsequent analysis of the secondary structure of the intracellular domain (Extended Data 1d) and
98 prediction of sequence disorder tendency (Extended Data 1c) and amino acid conservation
99 (Extended Data 1b) indicated that smMapZ forms a similar potential structure with spMapZ, and
100 both contain a predicted functional subdomain at the N-terminus of the cytoplasmic domain and
101 two subdomains of the extracellular domain.

102 Deletion of *smmapZ* (Δ*smmapZ*) led to shorter, irregularly shaped cells and mini-cells (Figure
103 1a, b), which is similar to the phenotype in *S. pneumoniae*. To assess the localisation pattern of
104 smMapZ, we fused enhanced green fluorescent protein (EGFP) to the N-terminus of smMapZ
105 under the control of the native promoter. Time-lapse imaging of EGFP-smMapZ (Figure 1c)
106 indicated that smMapZ formed a ring at the mid-cell and a pair of rings appeared as the cell
107 elongated. The distance between the two smMapZ rings increased as a function of cell length while
108 the distance between the smMapZ rings and their nearest cell pole did not change remarkably
109 (Figure 1d), suggesting that the smMapZ ring at the mid-cell split into two rings, which moved to
110 the cell equator of the new daughter cells. Interestingly, smMapZ with cytoplasmic domain deletion
111 (s*mmapZ*Δ*cyto*) resulted in loss of the ability to position at the constricting septum, resulting in
112 distribution throughout the cell membrane, whereas the extracellular domain null mutation
113 (*smmapZ*Δ*extra*) retained a septum localisation pattern (Figure 1e). This result differs from that of
114 spMapZ. Further multi-domain truncation analysis revealed that the predicted subdomain at the N-
115 terminus of the cytoplasmic domain and the subdomain tandem to the transmembrane domain
116 respond to such localisation patterns (Extended Data 2). Evolutionary tree analysis revealed that
117 smMapZ and spMapZ belong to different evolutionary branches (Figure s1).

118 **Deletion of *smmapZ* led to mislocalisation of the FtsZ ring.**

119 We next assessed the effect of smMapZ on the localisation of FtsZ. The red fluorescence
120 protein mCherry was used to label smMapZ and EGFP was fused to the C-terminus of FtsZ under
121 the control of an inducible promoter. Consistent with a previous report, FtsZ and smMapZ were
122 colocalised at the mid-cell in a newborn cell. Moreover, smMapZ was required for correct
123 localisation of the FtsZ ring, as 64% of FtsZ rings were unable to localise at the mid-cell in the
124 Δ*smmapZ* strain, while only 22.7% of FtsZ rings in the wild type (WT) strain were mislocalised
125 (Figure 2b). As the cell grew, the smMapZ ring split into a pair, which moved toward the cell
126 equator of the daughter cells before the FtsZ ring. A third smMapZ ring emerged at the division

site, constricting with the FtsZ ring. Subsequently, new FtsZ rings assembled, colocalising with the smMapZ rings of daughter cells (Figure 2a).

Deletion of *smmapZ* led to unconstrained treadmilling of FtsZ filaments in the Z-ring.

As a tubulin homologue in prokaryotic, the treadmilling motion of FtsZ filaments was confirmed recently[13, 14]. MapZ did not affect the polymerisation and GTPase activity of FtsZ[9], but deletion of MapZ did impact FtsZ ring localisation and constriction. Thus, we proposed that MapZ might control the treadmilling of FtsZ filaments. To confirm this hypothesis, we labelled FtsZ with a brighter green fluorescent protein, mNeongreen, and used total internal reflection fluorescence microscopy (TIRFM) to study the dynamics of FtsZ rings. The results revealed a periodic intensity fluctuation of the FtsZ ring (Figure 3a, Extended Data 3a). With kymography, we observed directional movement of the FtsZ ring (Figure 3b, Movie s1). In contrast with *E. coli,* in which only one FtsZ ring forms during a cell cycle, three FtsZ rings could be observed in the majority of *S. mutans* cells at a later stage of the cell cycle. Surprisingly, we observed translocation of FtsZ filaments from the middle (old) FtsZ ring to the nearby (new) FtsZ rings (Figure 3d, Movie s3), and the speed of translocation was similar to that of treadmilling inside the ring.

Interestingly, deletion of *smmapZ* led to highly unconstrained movement of FtsZ filaments (Figure 4a, Movie s5, s6), but did not perturb the treadmilling and translocation of FtsZ filaments (Figure 3a, b, d, Movie s2, s4) or alter the speed of treadmilling (Figure 3c), which suggests a crucial role of smMapZ in guiding the treadmilling movement of FtsZ filaments. Although the unconstrained FtsZ filaments could still form a ring-like structure as the cell grew, the angle of the FtsZ ring plane changed back and forth during FtsZ ring formation, which might ultimately lead to aberrant localisation of the Z ring. Nevertheless, once the Z ring was formed, the angle of the Z ring plane would no longer change (Extended Data 3b, Movie s5). We also noticed that deletion of *smmapZ* resulted in a decrease in chance to observe cells with three FtsZ rings (Extended Data 3c). By monitoring the complete process of emergence and disappearance of the three FtsZ ring structure, we discovered that the middle FtsZ ring in the Δ*smmapZ* strain only remained 5-6 min

153 after new FtsZ ring formation, exhibiting a shorter lifetime than the life time (>10 min) in the WT
154 strain (Figure 4b, Movie s7, s8). Analysis of the intensity trace also indicated that deleting *smmapZ*
155 led to a faster fluorescence decrease of the middle FtsZ ring than that in WT (Figure 4c). This
156 suggested that smMapZ might play a role in guiding the treadmilling and stabilising the constricting
157 FtsZ ring.

158 **smMapZ ring exhibits discontinuous and stable structure**

159 To understand how smMapZ guides the treadmilling of FtsZ filaments, we performed three-
160 dimensional structured illumination microscopy (3D-SIM) to study the structure of a Halotag-fused
161 smMapZ ($Halo_{JF549}$-smMapZ[16]) ring. The smMapZ ring exhibited a heterogeneous ring-like
162 structure at the division site (Figure 5a-c, Movie s11), similar to previously studied FtsZ, EzrA,
163 Pbp2[17], FtsA and ZipA[18]. Such discontinuous ring structures allow for direct observation of their
164 directional movements using single molecule TIRF imaging[13, 14]. Here, to study the dynamics of
165 smMapZ ring, we labelled smMapZ with mNeongreen for TIRF imaging. Interestingly, no
166 remarkable periodic motion of smMapZ was observed by intensity traces or kymograph analysis
167 (Figure 5d, Extended Data 4a, Movie s9), suggesting that the smMapZ ring is immobile. We further
168 observed the relative movement between smMapZ and FtsZ using a dual color assay. By labeling
169 smMapZ and FtsZ with EGFP and mScarlet-I, respectively, we revealed that the FtsZ ring exhibited
170 directional movement while the smMapZ ring showed no remarkable movement (Figure 5e).
171 Single molecule tracking allowed to measure the spatially specific dynamic features of targeted
172 molecules. Here, we labelled Halotag fused smMapZ with low concentrations (62.5 pM) of
173 HaloLigand-JF_{646} to monitor the motion of single smMapZ molecules. The results revealed two
174 populations of smMapZ molecules: (i) stationary and (ii) diffusive (Figure 5f, Movie s10). In a few
175 cases, we also observed one single smMapZ molecule switched between the two modes (Extended
176 Data 4b). We analysed the localisation pattern of stationary smMapZ molecules in 62 cells. In 38
177 cells that exhibited newborn cell length or three FtsZ ring structures, the stationary smMapZ
178 molecules co-localised with the FtsZ ring. In the rest 24 growing cells, the stationary smMapZ

179 molecules localised at the cell equator of the future daughter cells (Figure 5g, Extended Data 4c).
180 The low mobility of smMapZ molecules supports that smMapZ forms a stable ring structure.
181 However, as most single molecules were bleached in 2-3 min, single molecule trajectories were
182 insufficient to study the stability of the smMapZ ring over a longer period of time. Therefore, we
183 labelled smMapZ with mMaple3, a photoconvertable fluorescent protein that converts from green
184 fluorescence to red fluorescence under purple illumination[19]. Using TIRF illumination, we
185 photoconverted mMaple3-fused smMapZ molecules in the bottom portion of the ring using a 405
186 nm laser and monitored their movement every 3 min. The results showed that over a total duration
187 of 21 min, neither the position nor the intensity of the photoconverted smMapZ molecules changed
188 remarkably, indicating that the smMapZ ring is a stable structure and the exchange of smMapZ
189 molecules occurs at a very slow rate (Figure 5h, Extended Data 4d).

190 **Discussion**

191 Recently a membrane protein MapZ mediated FtsZ regulatory system was uncovered in *S.*
192 *pneumoniae,* which was shown to be conserved in *Streptococcaceae*. As a positive FtsZ regulator,
193 MapZ first binds to the division site forming a ring structure and then positions the FtsZ ring[9, 10].
194 Two recent studies[11, 12] gained insight into how MapZ marks the division site, but little work has
195 been focused on how MapZ controls the FtsZ ring structure. Here, our data suggested that MapZ
196 forms a stable heterogeneous ring structure at the division site, which may act as a track for the
197 treadmilling of FtsZ filaments (Figure 6). This is primarily demonstrated by the characterisation of
198 the smMapZ ring structure and FtsZ treadmilling in *S. mutans*.

199 smMapZ is essential for regular cell shape formation and proper localistion of the constricting
200 septum in *S. mutans*; it marks the division site prior to the FtsZ ring (Figure 2a). Deletion of
201 *smmapZ* results in a shorter, irregularly shaped cell, and a mislocalised FtsZ ring (Figure 1a, b,
202 Figure 2b).

203 To understand the mechanism by which the smMapZ ring affects the FtsZ ring localisation,
204 we focused on the treadmilling of FtsZ, which was confirmed recently. Similar to that in *E. coli*

205 and *B. subtilis,* the FtsZ ring in *S. mutans* demonstrated periodic fluctuations of intensity and a
206 directional motion in high temporal resolution imaging (Figure 3a, b, c, Extended Data 3a, Movie
207 s1). Interestingly, different from that in *E. coli* and *B. subtilis*, we observed translocation of FtsZ
208 from the middle ring to the newly formed FtsZ ring (Figure 3d). The translocation velocity was
209 similar to the treadmilling vecolity of FtsZ filaments inside the ring. Considering that the
210 translocated FtsZ would participate in new ring formation, it is reasonable to note that such kind of
211 FtsZ translocation is a functional process rather than abnormal localisation. The translocation of
212 FtsZ also supports the view that the FtsZ ring consists of multiple protofilaments, thereby
213 demonstrating a bead-like structure or discontinuous clusters[17, 18, 20, 21].

214 Further, we revealed that deletion of *smmapZ* resulted in unconstrained movement of FtsZ
215 filaments and an unstable plane of the FtsZ ring (Figure 4a; Extended Data 3b), suggesting that the
216 smMapZ ring may play a role in restricting and guiding FtsZ treadmilling. This can also explain
217 why deletion of MapZ leads to an irregular cell shape and minicell formation. Consistent with a
218 previous report[9], we observed a lower proportion of cells harbouring the FtsZ dumbbell structure
219 in the Δ*smmapZ* strain compared to the WT cells (Extended Data 3c). This was probably due to the
220 shorter lifetime of the middle FtsZ ring in the Δ*smmapZ* strain (Figure 4b, c). We speculate that the
221 shorter lifetime was caused by an increase in FtsZ translocation (Movie s5); however, we cannot
222 exclude the possibility that it may have been due to premature constriction of the FtsZ ring, as
223 previously described[9].

224 We characterised the smMapZ ring structure to understand how it guides the treadmilling of
225 FtsZ filaments. The discontinued ring-like structure of smMapZ was uncovered by 3D-SIM (Figure
226 5a-c). However, unlike FtsZ, FtsA and Pbp2B[14], the smMapZ ring or single smMapZ molecules
227 did not show remarkable directional movement around the short cell axis (Figure 5d and Extended
228 Data 3a). Thus, we hypothesise that smMapZ localisates at the division site prior to FtsZ and forms
229 a stable heterogeneous ring-like structure (Figure 5g, h; Extended Data 3c, d). This stable ring
230 structure acts as a track for FtsZ treadmilling (Figure 5e). However, we noticed that FtsZ still

231 formed a Z ring in the Δ*smmapZ* strain. The change of plane angle of the FtsZ ring often happened
232 at the early stage of FtsZ ring formation but not in the constricting stage. Thus, we propose that the
233 track role of MapZ only functions at the early stage of FtsZ ring formation, and other proteins also
234 participate in the stablisation of FtsZ treadmilling after Z ring formation, possibly including ErZA,
235 a spectrin like protein[22], which has been reported to interact with FtsZ and is required for correct
236 localisation of the FtsZ ring[23].

237 In summary, our study revealed the "track" role of smMapZ in FtsZ treadmilling, providing
238 new insight into the mechanism of the MapZ-mediated FtsZ regulatory system. Considering the
239 similar functions of smMapZ with that of spMapZ, we believe this does not only exist in *S. mutans*,
240 but also in other MapZ-conserved bacteria.

241

242

243

244 **Material and methods**

245 **Bacterial strains, plasmid and mutation construction, and culture conditions**

246 *S. mutans* standard strain UA159 and all derived strains used in this study are listed in Table
247 1. To generate the *S. mutans* mutations (gene deletion and fluorescent protein fusion), we used a
248 counter-selectable system called IFDC2 (provided by Zhoujie Xie). The transformation procedure
249 was performed as previously described[24]. Briefly, the overnight culture grown in Todd–Hewitt
250 medium supplemented with 0.3% yeast extract (THY; QinDao Wei si, China) was diluted (1:20)
251 in the same medium and incubated for 2–3 h (OD_{600} 0.2–0.3). Overlapping PCR reaction (5 μl) and
252 0.5 μl of CSP (1 μg/μl stock) were added to 500 μl of culture and incubated for 2 h. To select
253 antibiotic-resistant colonies, brain heart infusion (BHI; Difco Laboratories, Detroit, MI, USA) agar
254 plates were supplemented with 12-μg/ml erythromycin (Sigma-Aldrich, St. Louis, MO, USA).
255 Selection of the second transformation was performed on BHI plates supplemented with 4-mg/ml
256 p-cl-Phe (Sigma-Aldrich). For snapshot imaging, *S. mutans* strains were aerobically cultured in

257 THY at 37°C. For time-lapse imaging, the strains were cultured in a chemically defined medium[25]
258 supplemented with 0.3% yeast extract (C + Y). A final concentration of 10 mg/ml xylose was added
259 to the culture medium to induce the expression of Pzx9 and Pzx10[26] (provided by Jiezhou Xie).

260 **Sample preparation for snapshot imaging**

261 An overnight culture grown in THY medium was diluted (1:100) in the same medium, and
262 incubated at 37°C aerobically to OD_{600} 0.4–0.5 (7 h). The culture was diluted again (1:100) in THY
263 and grown at 37°C aerobically to OD_{600} 0.1–0.2 (5 h). Cells were harvested by centrifugation at
264 1,500 × *g* for 3 min, washed three times with 1× phosphate-buffered saline (PBS), and resuspended
265 in 1× PBS. The bacteria were loaded between a gel pad (1× PBS supplemented with 1.5% low
266 melting agarose) and coverslip (Fisher 24 × 50, No. 1). For FtsZ imaging, spectinomycin was added
267 to all cultures at a final concentration of 1 mg/ml. D (+) xylose (Sigma-Aldrich) was added before
268 the last round of dilution at 10 mg/ml.

269 **Sample preparation for 3D-SIM imaging**

270 JF_{549} dye (500 nM; provided by Luke Lavis) was added into the culture at OD_{600} 0.1–0.2,
271 incubated for 15 min at 37°C, washed once with 1× PBS, fixed in 4% paraformaldehyde for 15 min
272 at room temperature, and washed twice with 1× PBS. Resuspended cells were loaded between the
273 coverslip (Fisher 24 × 50, No. 1.5) and gel pad.

274 **Sample preparation for time-lapse imaging**

275 *EGFP_smMapZ and mMaple3_smMapZ.* An overnight culture grown in THY medium was
276 diluted (1:100) in C + Y medium. After two dilutions, the culture at OD_{600} 0.1–0.2 was added to a
277 gel pad (C + Y medium supplemented with 1.5% low melting agarose) on a glass slide, and a
278 coverslip was added. Rectangular 3M double-sided tape was used to seal the coverslip and glass
279 slide.

280 *HaloJF$_{646}$_smMapZ.* JF_{646} dye (62.5 pM) was added into the culture at OD_{600} 0.1–0.2,
281 incubated for 15 min at 37°C and washed once with pre-warmed fresh C + Y medium. Resuspended
282 cells were loaded between the coverslip and the gel pad.

283 *Imaging of FtsZ_mNeongreen*. Spectinomycin was added to all cultures at a final
284 concentration of 1 mg/ml. D (+) xylose was added at 10 mg/ml before the last round of dilution.

285 **Slide preparation**

286 Coverslips were cleaned with Piranha solution (30% H_2O_2: 98% H_2SO_4 v:v = 1:3 at 90°C for 30
287 min), washed with Milli-Q water, stored in filtered Milli-Q water, and dried with high purity
288 nitrogen before use

289 **Snapshot imaging of smMapZ and FtsZ**

290 The samples were visualised on an N-STORM (Nikon, Tokyo, Japan) system equipped with
291 a 100× oil TIRF objective (Nikon PLAN APO, 1.49 NA), Andor-897 EMCCD (Andor, Belfast,
292 Northern Ireland), the perfect focus system (Nikon), a laser source (405, 488, 561, and 647 nm)
293 and 1.5× magnification optics. Images were collected with Nis-Elements AR software (Nikon). For
294 EGFP_smMapZ and mCherry_smMapZ, 300 frames were collected with a 100 ms exposure time.
295 For FtsZ_EGFP, 50 frames were collected with a 100 ms exposure time.

296 **Time-lapse imaging of EGFP_smMapZ and mMaple3_smMapZ**

297 Time-lapse observation of EGFP_smMapZ was performed with a DeltaVision OMX SR (GE
298 Healthcare, Little Chalfont, UK) system equipped with a 1.42 NA 60× oil objective (Olympus,
299 Tokyo, Japan), laser source (405, 488, 561, and 642 nm), four sCOMS, and an environment control
300 system. Using the OMX Acquisition software, the images were collected with a 60 ms exposure
301 time, with 5 min intervals at 37°C.

302 Time-lapse imaging of mMaple3_smMapZ was performed with an N-STORM microscope
303 equipped with a live cell instrument. A laser at 405 nm was used to photoconvert the mMaple3 to
304 the red state with an initial exposure time of 300 ms. Then, a 561 nm laser was used to excite the
305 red state mMaple3 with a 400 ms exposure time, and a 488 nm laser was used for the green state
306 with a 300 ms exposure time.

307 **3D-SIM imaging of HaloJF$_{549}$_smMapZ**

308 Super-resolution 3D-SIM imaging was performed with a DeltaVision OMX SR system, with
309 a 10 ms exposure time and 50% transmission. The 3D-SIM raw data were reconstructed with
310 SoftWoRx 6.0 (Applied Precision, Issaquah, WA, USA) using a Wiener filter setting of 0.001 and
311 a channel that specifically measured optical transfer functions. The immersion oil was optimised
312 to 1.518.
313

314 **Imaging of the dynamics of FtsZ_mNeongreen, mNeongreen_smMapZ and**
315 **HaloJF646_smMapZ**

316 The images were collected by near-TIRF illumination on an N-STORM microscope.
317 Exposure time was 0.165 s, interval time was 0.495 s, and mNeongreen was excited by the 488 nm
318 laser. The images were captured at room temperature. For the single molecular track of HaloJF646-
319 smMapZ, exposure time was 0.1 s, and the interval time was 0.5 s. The 647 nm laser was used to
320 excite the JF646 dye.

321 **Data analysis**

322 *Localisation of smMapZ*. The averaged image stacks were obtained, and Snapshot analysis
323 accomplished, with ImageJ software (NIH, Bethesda, MD, USA). Cell outlines and corresponding
324 fluorescence signals were manually detected and analysed using MicrobeTracker[27] and custom
325 MATLAB (MathWorks, Natick, MA, USA) codes. Information regarding the cell length of WT
326 and ΔsmMapZ was extracted and the graph was generated in Microsoft Excel software (Microsoft
327 Corp., Redmond, WA, USA). To compare the distance between the two outer rings, and between
328 the smMapZ ring and the cell pole, we manually eliminated the cell in which only one ring structure
329 could be observed, then the data were calculated with a custom MATLAB script and plotted in
330 Excel. To sort the fluorescence intensity of the smMapZ truncations as a function of cell length,
331 averaged images were deconvoluted using Huygens and subsequently analysed using Coli-
332 Inspector running under the ImageJ plugin ObjectJ (http://simon.bio.uva.nl/objectj/), as previously
333 described[11].

334

335 The analysis of periodic intensity fluctuations of the Z ring and treadmilling were performed
336 in Fiji (http://fiji.sc/). First, drift correction of the time-lapse imaging was performed using series
337 registration based on the Fiji plugin Descriptor. We selected a medium detection brightness and
338 six-pixel for detection size; the type of detection was set as minima and maxima, and the rest were
339 set as default values. After drift correction, a 3 × 3 pixel (~320 nm) region of interest was chosen
340 inside the Z ring, and the Z-axis profile was plotted with Fiji to show the periodic intensity
341 fluctuations. For analysis of FtsZ treadmilling, the images were resized to 26 nm/pixel with the
342 bicubic method, and a segmented line (line width is 11) was drawn inside the Z ring, parallel to its
343 long axis, and a multiple kymograph plugin was used to demonstrate movement. The velocity of
344 treadmilling was calculated based on the kymograph using the macro "read velocities from tsp" as
345 described in the manual.

346 *Single particle tracking*. The Fiji plugin TrackMate (http://imagej.net/TrackMate) was used
347 to analyse the trajectory of single molecules of smMapZ. We selected the LoG detector and set 0.4
348 μm as the estimated blob diameter. The LAP Tracker function, with a 0.5 μm maximum distance
349 for frame-to-frame linking, was employed to complete the tracking. The trajectory data were
350 exported; further analysis of logD was carried out in R studio (R Development Core Team, Vienna,
351 Austria) with a custom script. The two-status analysis of single trajectory was performed in
352 MATLAB with the HMM-Bayes procedure[28] , as previously described.

353 *smMapZ sequence analysis*. To identify smMapZ, we selected spMapZ as the query sequence
354 and used BLAST (https://blast.ncbi.nlm.nih.gov/Blast.cgi) to search the genome of *S. mutans*. The
355 two sequences were aligned with SnapGene software (GSL Biotech LLC, Chicago, IL, USA). The
356 transmembrane domain was predicted using TMHMM Server v. 2.0
357 (http://www.cbs.dtu.dk/services/TMHMM/). Network Protein Sequence Analysis[29] (http://npsa-
358 pbil.ibcp.fr) was used to predict the secondary structure of the cytoplasmic domain of smMapZ as

359 previously described. In total, 150 protein sequences were selected to determine amino acid
360 conservation using the Consurf web server[30] (http://consurf.tau.ac.il/2016/). Prediction of sequence
361 disordered tendency was performed with IUPred[31] (http://iupred.enzim.hu/).
362

363 **ACKNOWLEDGEMENTS**

364 This work was funded by Peking University's 985 Grant and the National Natural Science
365 Foundation of China (No. 30973317, 31271423, and 21390412). We thank Zhoujie Xie (Institute
366 of Microbiology, CAS) for his assistance in the construction of the mutations and Chunyan Shan
367 (The Core Imaging Facility of Peking University) for her help on DeltaVision OMX. We thank He
368 Yu, Professor Can Xie and ShuJin Luo (School of Life Sciences, Peking University) for their help
369 with analysis of evolution tree.
370

371 1. Bi EF, Lutkenhaus J. FtsZ ring structure associated with division in Escherichia coli.
372 *Nature* 1991, **354**(6349)**:** 161-164.
373
374 2. Adams DW, Errington J. Bacterial cell division: assembly, maintenance and disassembly
375 of the Z ring. *Nature reviews Microbiology* 2009, **7**(9)**:** 642-653.
376
377 3. Rowlett VW, Margolin W. The bacterial Min system. *Current biology : CB* 2013, **23**(13)**:**
378 R553-556.
379
380 4. Wu LJ, Errington J. Nucleoid occlusion and bacterial cell division. *Nature reviews*
381 *Microbiology* 2011, **10**(1)**:** 8-12.
382
383 5. Rodrigues CDA, Harry EJ. The Min System and Nucleoid Occlusion Are Not Required for
384 Identifying the Division Site in Bacillus subtilis but Ensure Its Efficient Utilization. *Plos*
385 *Genet* 2012, **8**(3).
386
387 6. Thanbichler M, Shapiro L. MipZ, a spatial regulator coordinating chromosome
388 segregation with cell division in Caulobacter. *Cell* 2006, **126**(1)**:** 147-162.
389

390 7. Treuner-Lange A, Aguiluz K, van der Does C, Gomez-Santos N, Harms A, Schumacher D*,*
391 *et al.* PomZ, a ParA-like protein, regulates Z-ring formation and cell division in
392 Myxococcus xanthus. *Mol Microbiol* 2013, **87**(2)**:** 235-253.

393
394 8. Willemse J, Borst JW, de Waal E, Bisseling T, van Wezel GP. Positive control of cell
395 division: FtsZ is recruited by SsgB during sporulation of Streptomyces. *Genes &*
396 *development* 2011, **25**(1)**:** 89-99.

397
398 9. Fleurie A, Lesterlin C, Manuse S, Zhao C, Cluzel C, Lavergne JP*, et al.* MapZ marks the
399 division sites and positions FtsZ rings in Streptococcus pneumoniae. *Nature* 2014,
400 **516**(7530)**:** 259-262.

401
402 10. Holeckova N, Doubravova L, Massidda O, Molle V, Buriankova K, Benada O*, et al.* LocZ is
403 a new cell division protein involved in proper septum placement in Streptococcus
404 pneumoniae. *mBio* 2014, **6**(1)**:** e01700-01714.

405
406 11. Manuse S, Jean NL. Structure-function analysis of the extracellular domain of the
407 pneumococcal cell division site positioning protein MapZ. *Nature communications* 2016,
408 **7:** 12071.

409
410 12. van Raaphorst R, Kjos M, Veening JW. Chromosome segregation drives division site
411 selection in Streptococcus pneumoniae. *Proc Natl Acad Sci U S A* 2017, **114**(29)**:** E5959-
412 e5968.

413
414 13. Yang X, Lyu Z. GTPase activity-coupled treadmilling of the bacterial tubulin FtsZ
415 organizes septal cell wall synthesis. *Science* 2017, **355**(6326)**:** 744-747.

416
417 14. Bisson-Filho AW, Hsu YP. Treadmilling by FtsZ filaments drives peptidoglycan synthesis
418 and bacterial cell division. *Science* 2017, **355**(6326)**:** 739-743.

419
420 15. Garcia PS, Simorre JP, Brochier-Armanet C, Grangeasse C. Cell division of Streptococcus
421 pneumoniae: think positive! *Current opinion in microbiology* 2016, **34:** 18-23.

422
423 16. Grimm JB, English BP, Chen J, Slaughter JP, Zhang Z, Revyakin A*, et al.* A general method
424 to improve fluorophores for live-cell and single-molecule microscopy. *Nature methods*
425 2015, **12**(3)**:** 244-250, 243 p following 250.

426
427 17. Strauss MP, Liew ATF, Turnbull L, Whitchurch CB, Monahan LG, Harry EJ. 3D-SIM Super
428 Resolution Microscopy Reveals a Bead-Like Arrangement for FtsZ and the Division
429 Machinery: Implications for Triggering Cytokinesis. *Plos Biology* 2012, **10**(9).

430

431 18. Rowlett VW, Margolin W. 3D-SIM Super-resolution of FtsZ and Its Membrane Tethers in
432 Escherichia coli Cells. *Biophysical Journal* 2014, **107**(8)**:** L17-L20.

433
434 19. Wang S, Moffitt JR, Dempsey GT, Xie XS, Zhuang X. Characterization and development of
435 photoactivatable fluorescent proteins for single-molecule-based superresolution
436 imaging. *Proc Natl Acad Sci U S A* 2014, **111**(23)**:** 8452-8457.

437
438 20. Guo F, Tao H, Buss J, Coltharp C, Hensel Z, Jie X. In Vivo Structure of the E. coli FtsZ-ring
439 Revealed by Photoactivated Localization Microscopy (PALM). *PloS one* 2010, **5**(9).

440
441 21. Buss J, Coltharp C, Huang T, Pohlmeyer C, Wang S-C, Hatem C*, et al.* In vivo organization
442 of the FtsZ-ring by ZapA and ZapB revealed by quantitative super-resolution microscopy.
443 *Molecular Microbiology* 2013, **89**(6)**:** 1099-1120.

444
445 22. Cleverley RM, Barrett JR, Basle A, Bui NK, Hewitt L, Solovyova A*, et al.* Structure and
446 function of a spectrin-like regulator of bacterial cytokinesis. *Nature communications*
447 2014, **5:** 5421.

448
449 23. Jorge AM, Hoiczyk E, Gomes JP, Pinho MG. EzrA contributes to the regulation of cell size
450 in Staphylococcus aureus. *PloS one* 2011, **6**(11)**:** e27542.

451
452 24. Xie Z, Okinaga T, Qi F, Zhang Z, Merritt J. Cloning-independent and counterselectable
453 markerless mutagenesis system in Streptococcus mutans. *Applied and environmental*
454 *microbiology* 2011, **77**(22)**:** 8025-8033.

455
456 25. van de Rijn I, Kessler RE. Growth characteristics of group A streptococci in a new
457 chemically defined medium. *Infection and immunity* 1980, **27**(2)**:** 444-448.

458
459 26. Xie Z, Qi F, Merritt J. Development of a tunable wide-range gene induction system useful
460 for the study of streptococcal toxin-antitoxin systems. *Applied and environmental*
461 *microbiology* 2013, **79**(20)**:** 6375-6384.

462
463 27. Sliusarenko O, Heinritz J, Emonet T, Jacobs-Wagner C. High-throughput, subpixel
464 precision analysis of bacterial morphogenesis and intracellular spatio-temporal
465 dynamics. *Mol Microbiol* 2011, **80**(3)**:** 612-627.

466
467 28. Monnier N, Barry Z, Park HY, Su KC, Katz Z, English BP*, et al.* Inferring transient particle
468 transport dynamics in live cells. *Nature methods* 2015, **12**(9)**:** 838-840.

469
470 29. Combet C, Blanchet C, Geourjon C, Deleage G. NPS@: network protein sequence
471 analysis. *Trends in biochemical sciences* 2000, **25**(3)**:** 147-150.

30. Landau M, Mayrose I, Rosenberg Y, Glaser F, Martz E, Pupko T*, et al.* ConSurf 2005: the projection of evolutionary conservation scores of residues on protein structures. *Nucleic acids research* 2005, **33**(Web Server issue)**:** W299-302.

31. Dosztanyi Z, Csizmok V, Tompa P, Simon I. IUPred: web server for the prediction of intrinsically unstructured regions of proteins based on estimated energy content. *Bioinformatics* 2005, **21**(16)**:** 3433-3434.

Figure legends

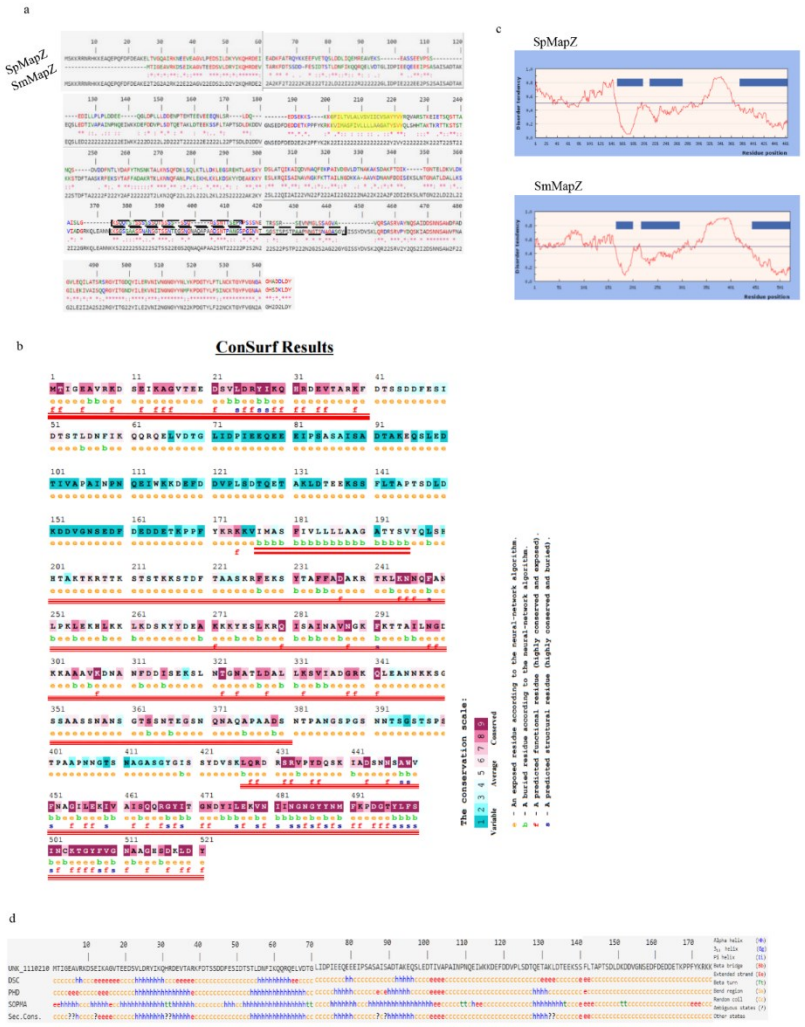

484 Extended Data 1. **Sequence analysis of *Stretococcus mutans* MapZ (smMapZ)**. (a) Alignment
485 of smMapZ and *Streptococcus pneumoniae* MapZ (spMapZ). The transmembrane domain is
486 marked with a yellow box. SR linker is indicated by the dotted rectangle. (b) Amino acid
487 conservation of smMapZ. Red lines indicate conserved regions. (c) Predicted disorder tendency
488 of smMapZ and spMapZ. (d) Secondary structure prediction of the cytoplasmic domain of
489 smMapZ.
490
491

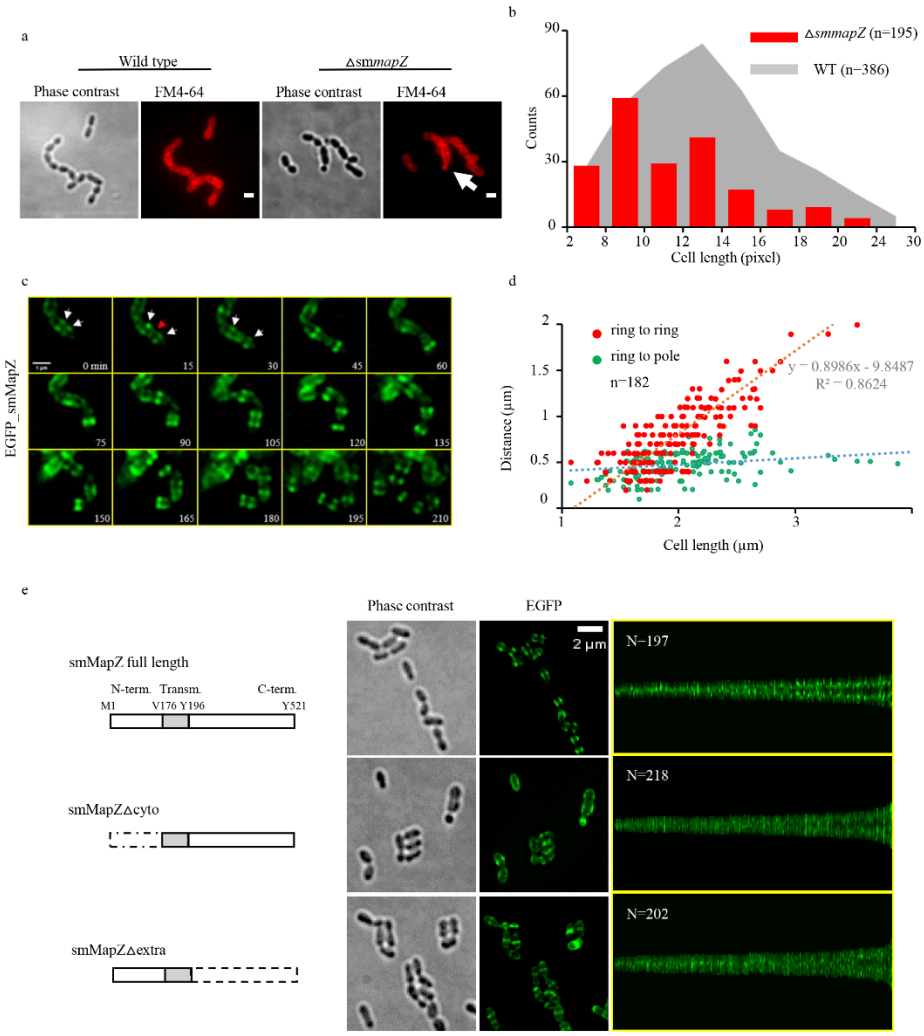

492 Figure 1. **Characterisation of a MapZ homologue in *S. mutans* (smMapZ)**. (a) Cell shape of
493 wild type (WT) and deletion of *smmapZ* (Δ*smmapZ*). Membrane was stained with FM4-64. A

494 minicell is indicated by the white arrow. Scale bar, 1 μm. (b) Analysis of cell length of WT and
495 Δ*smmapZ*. (c) Live cell imaging of enhanced green fluorescent protein (EGFP) smMapZ. White
496 arrows indicate the split smMapZ rings, and the red arrow indicates the third smMapZ ring. (d)
497 Analysis of the distance between the two outer rings, and between the ring and the nearest pole.
498 (e) Localisation pattern of WT smMapZ, smMapZ with cytoplasmic domain deletion
499 (smMapZΔcyto), and the extracellular domain null mutation (smMapZΔextra). A schematic of
500 the mutations is shown on the left, cell shape and EGFP signals in the middle, and corresponding
501 maps of fluorescence intensity (sorted by cell length) on the right.
502
503
504

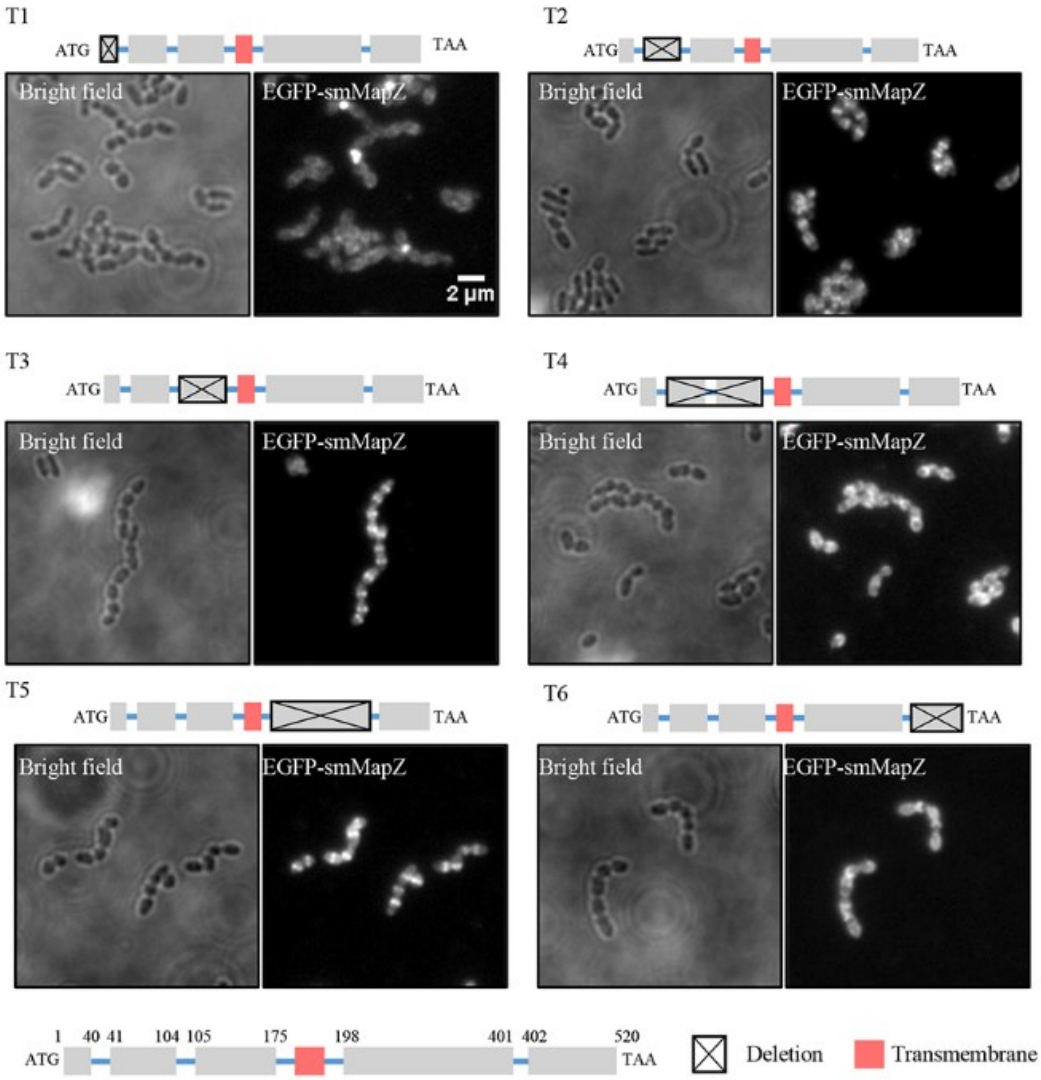

Extended Data 2. **Localisation of smMapZ truncations.** The potential subdomains of the cytoplasmic domain were predicted based on its secondary structure. The potential subdomains of the extracellular domain were predicted based on amino acids conservation and disorder tendency analysis.

513

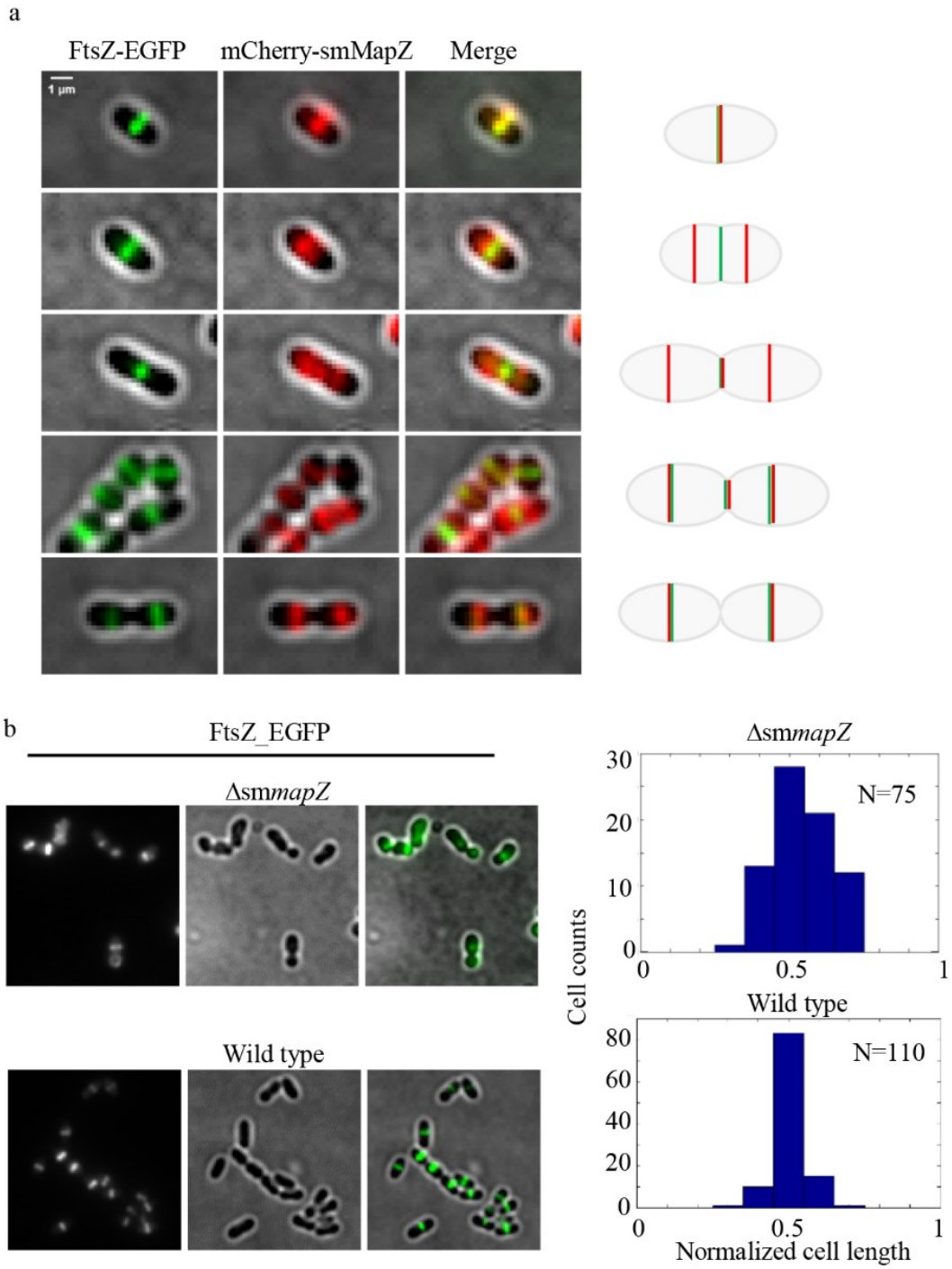

514 Figure 2. **Effect of smMapZ on FtsZ localisation**. (a) Dual colour imaging of smMapZ and FtsZ

515 in different stages of the cell cycle. (b) Localisation of FtsZ in WT and Δ*smmapZ*. Cell shape

516 observed by phase contrast microscopy and fluorescence of EGFP are shown on the left, and

517 statistical analysis of FtsZ ring position is shown on the right.

518

519

520

521

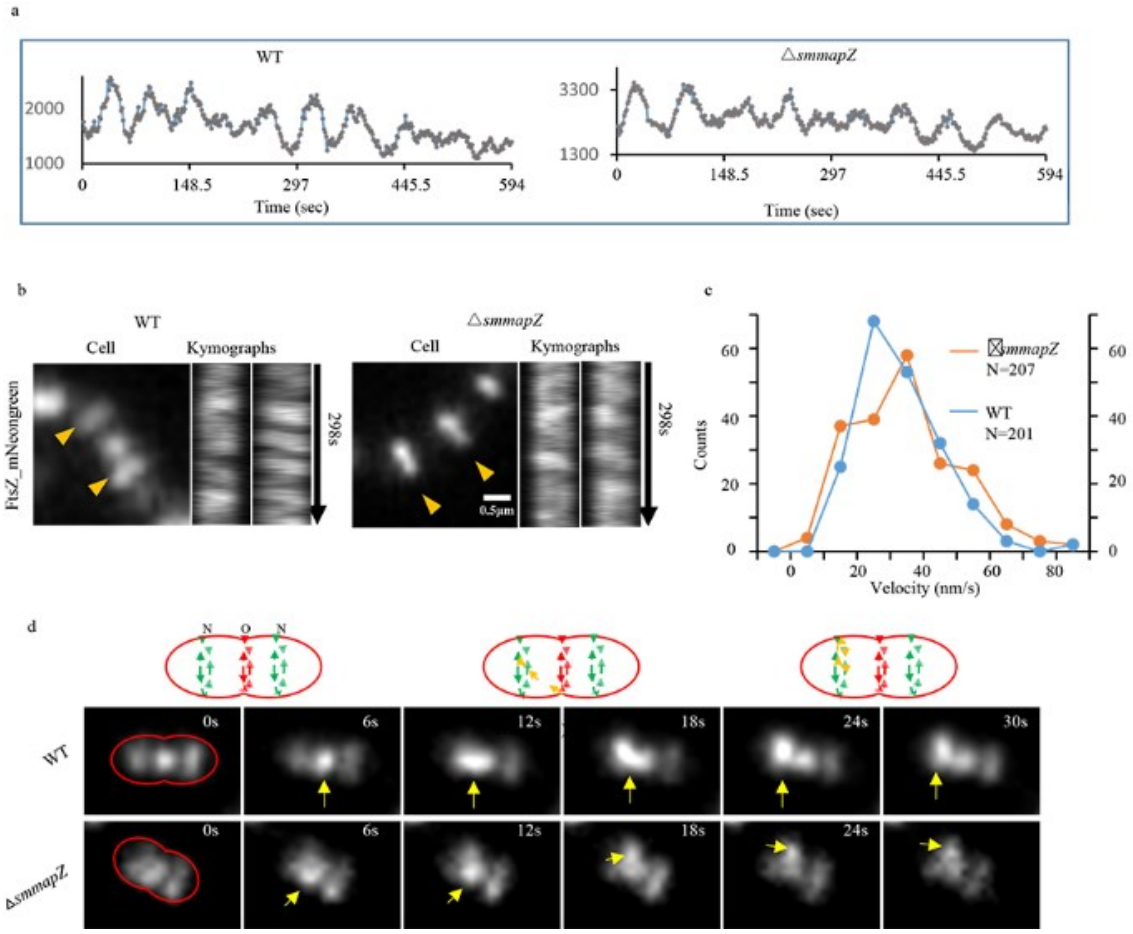

522

523 Figure 3. **FtsZ shows directional movement on smMapZ**. (a) Typical periodic fluctuation of the

524 FtsZ ring in WT and Δ*smmapZ*. (b) Typical direct movement of FtsZ in WT and Δ*smmapZ*. (c)

525 Distribution of velocity of FtsZ movement inside the rings. (d) Translocation of the FtsZ filament.

526 Schematics are shown above. “O” refers to the old ring and “N” refers to newly formed rings.

527 Fluorescence images are shown below. The red line indicates cell shape, and yellow arrows mark

528 the initiation of translocation.

529

530

531

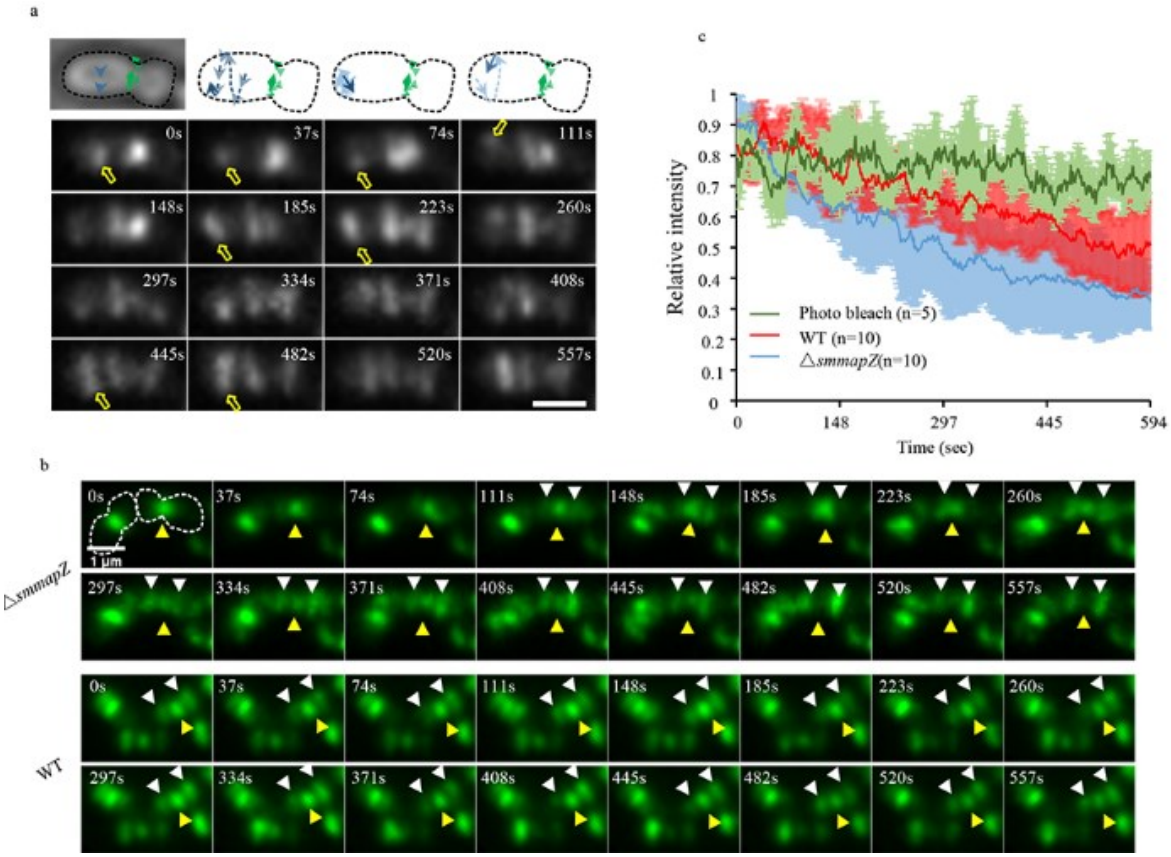

532

533

534 Figure 4. **Deletion of *smmapZ* lead to unconstrained FtsZ treadmilling**. (a) Unconstrained

535 movement of the FtsZ filaments in Δ*smmapZ*. Diagrams of the first four snapshots are shown in

536 the upper panel, and the cell shape in bright field, marked by a dotted line, is shown in the upper

537 left. In the diagrams, the dark blue arrows indicate the position and direction of movement of

538 FtsZ filaments, and light blue arrows indicate the movement path of FtsZ. In snapshots of the

539 time-lapse imaging shown below, yellow arrows mark the position of FtsZ and the change of

plane of the FtsZ ring. (b) Snapshots of the time-lapse imaging of three FtsZ ring structures in WT and Δ*smmapZ*. White arrows mark the newly formed FtsZ ring position and yellow arrows show the position of the old FtsZ ring. (c) Fluorescence intensity traces of the old FtsZ ring as a function of time.

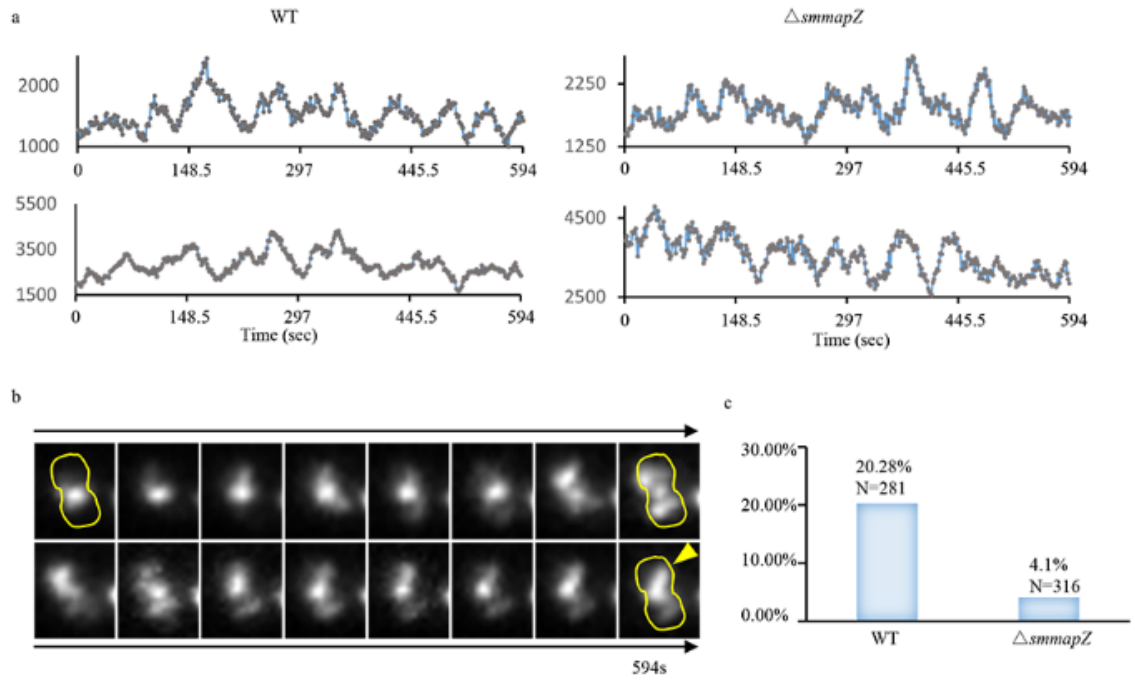

Extended Data 3. **Additional results of the effect of smMapZ on FtsZ treadmilling.** (a) Two representative fluorescence intensity fluctuations of FtsZ_mNeongreen in WT and Δ*smmapZ*. (b) Abnormal FtsZ ring plane and division septum. (c) Proportion of three FtsZ ring structures in WT and Δ*smmapZ*.

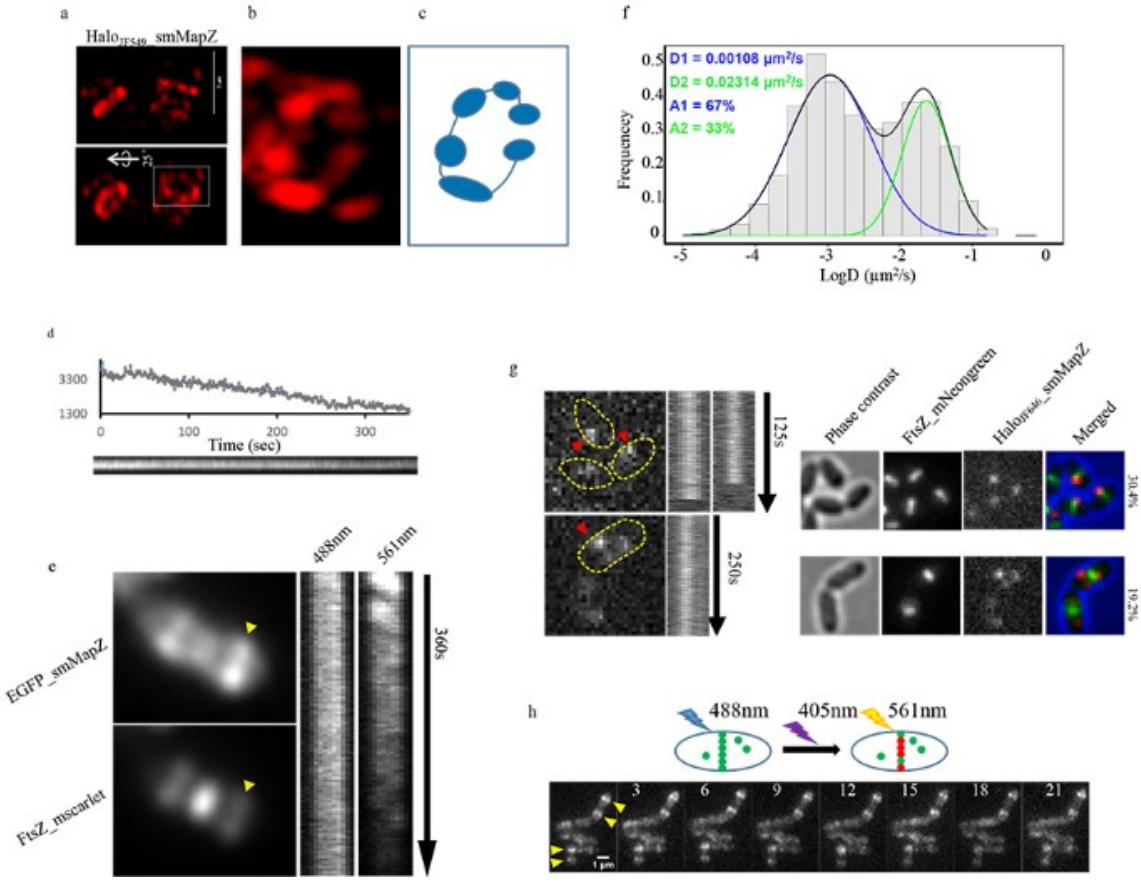

Figure 5. **Characterisation of the smMapZ ring**. (a) Three-dimensional structured illumination microscopy of HaloJF$_{549}$_smMapZ. (b) Heterogeneous ring structure of smMapZ in the box region of (a). (c) Cartoon of the heterogeneous ring structure in (b). (d) Intensity trace and kymograph analysis of mNeongreen_smMapZ. (e) Dual colour analysis of the movement of FtsZ and smMapZ. (f) Distribution of logD of single molecule tracking of smMapZ. D is the diffusion coefficient. The Gaussian fitting curve, the average D, and area of the two populations are shown. (g) Kymograph analysis of representative constrained molecules (left) and the localised relationship between the FtsZ ring in the newborn (upper) and the grown (lower) cells (right). (h) Snapshots of the time-lapse imaging of mMaple3_smMapZ. The smMapZ ring structure is marked by yellow arrows.

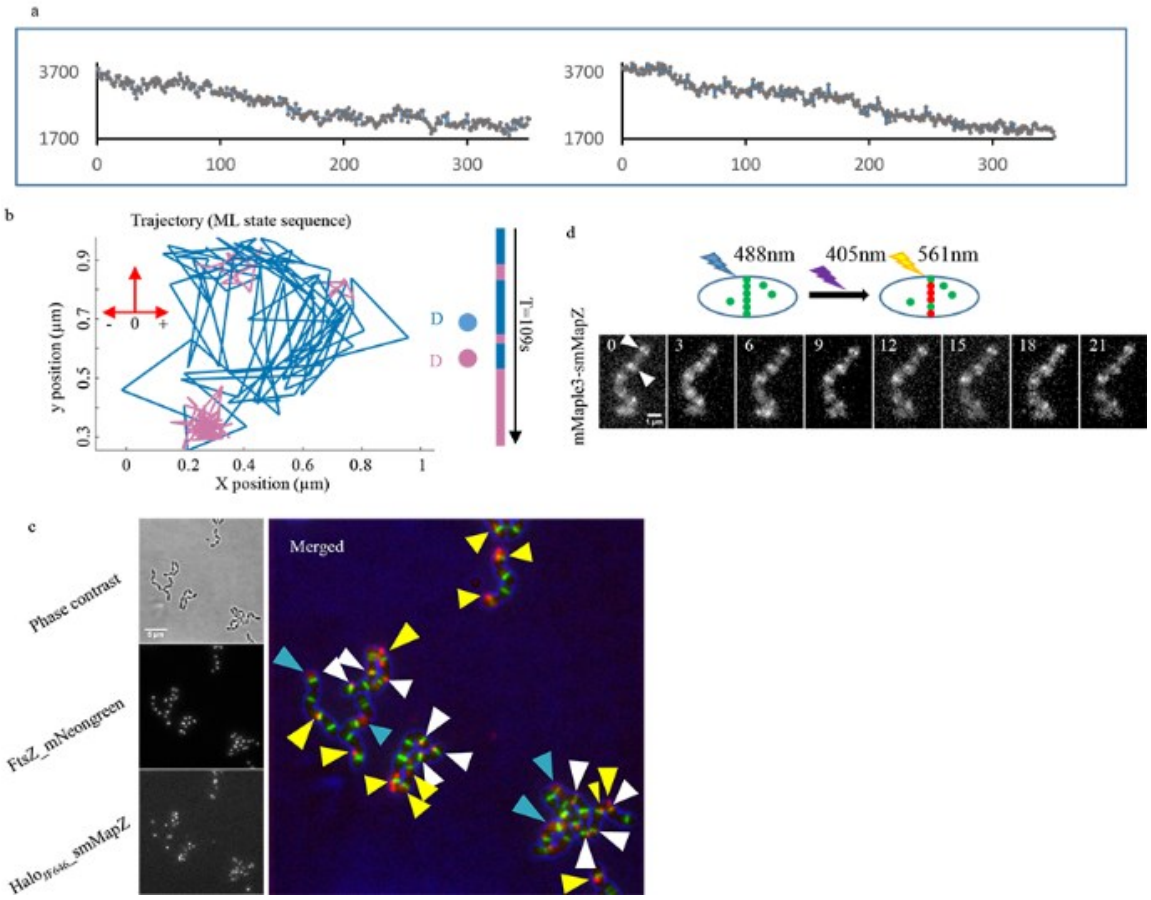

Extended Data 4. **Additional characterisation of the smMapZ ring.** (a) Additional intensity traces of mNeongreen_smMapZ. (b) Hidden Markov model-Bayes analysis of the trajectory with a combination of immobilisation and diffusion. Two diffusive statuses (D-D) were predicted, and blue and pink annotations represent the higher and lower diffusion coefficient status, respectively. (c) Typical images of the relationship between smMapZ molecules and FtsZ rings. The average of the first 50 frames of Halo$_{JF646}$_smMapZ is shown. White arrows mark the cells in which immobilised smMapZ molecules co-localise with the FtsZ ring. Yellow arrows mark the cells in which immobilised smMapZ molecules do not co-localise with the FtsZ rings. Blue arrows mark the cells in which smMapZ molecules are diffuse.

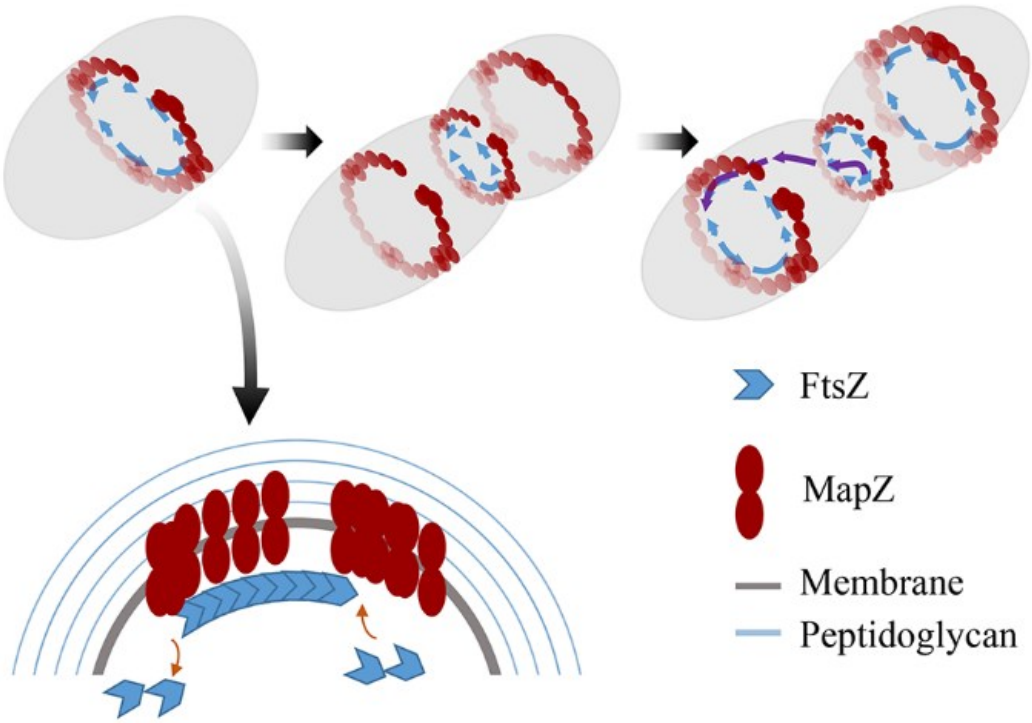

Figure 6. **Model of smMapZ guiding the treadmilling of FtsZ**. smMapZ forms a stable heterogeneous ring-like structure at the division site. The stable ring acts as a track for the treadmilling of FtsZ and, as the cell grows, this stable smMapZ ring moves to the future division site of daughter cells before the FtsZ ring. Newly formed FtsZ will move along the stable ring, and the translocated FtsZ filaments will also participate in new ring formation.

596

597 Table 1

S. mutans strains	Genotype and description	reference
UA159	S. mutans str UA159	Gift from Yifei Zhang, Central Laboratory of School and Hospital of Stomatology, Peking University,China
ΔsmmapZ	UA159; ΔSmu473	This study
EGFP_smMapZ	UA159; Smu473::EGFP-Smu473	This study
mCherry_smMapZ	UA159; Smu473::mCherry-Smu473	This study
Halo_smMapZ	UA159; Smu473::Halo tag-Smu473	This study
mNeongreen_smMapZ	UA159; Smu473::mNeongreen-Smu473	This study
EGFP_smMapZΔcyto	UA159; Smu473::EGFP-Smu473-Δcytoplasmic domain	This study
EGFP_smMapZΔextra	UA159; Smu473::EGFP-Smu473-Δextracellular domain	This study
EGFP_smMapZΔcyto(1-40)	UA159; Smu473::EGFP-Smu473-ΔM1-F40	This study
EGFP_smMapZΔcyto(41-104)	UA159; Smu473::EGFP-Smu473-ΔD41-A104	This study
EGFP_smMapZΔcyto(105-175)	UA159; Smu473::EGFP-Smu473-ΔP105-K175	This study
EGFP_smMapZΔcyto(41-175)	UA159; Smu473::EGFP-Smu473-ΔD41-K175	This study
EGFP_smMapZΔextra(198-401)	UA159; Smu473::EGFP-Smu473-ΔQ198-T401	This study
EGFP_smMapZΔextra(402-521)	UA159; Smu473::EGFP-Smu473-ΔP402-Y521	This study
FtsZ-EGFP	UA159; Pzx10::FtsZ-EGFP, Str^R	This study
FtsZ-mNeongreen	UA159; Pzx9::FtsZ-mNeongreen, Str^R	This study
FtsZ-mScarlet	UA159; Pzx9::FtsZ-mScarlet-I, Str^R	This study
ΔsmmapZ FtsZ-EGFP	UA159; ΔSmu473 Pzx10::FtsZ-EGFP, Str^R	This study
mCherry_smMapZ FtsZ-EGFP	UA159; Smu473::mCherry-Smu473 Pzx10::FtsZ-EGFP, Str^R	This study
EGFP_smMapZ FtsZ-mScarlet	UA159; Smu473::EGFP-Smu473 Pzx9::FtsZ-mScarlet-I, Str^R	This study
Halo_smMapZ FtsZ-mNeongreen	UA159; Smu473::Halo tag-Smu473 FtsZ-mNeongreen, Str^R	This study

598 **Supplementary**

599 **Figure s1: Evolutionary tree analysis of smMapZ and spMapZ in *Streptococcaceae.***

600 **Movie s1. Directional movement of FtsZ inside the Z ring in WT cells.**

601 **Movie s2. Directional movement of FtsZ inside the Z ring in △*smmapZ* cells.**

602 **Movie s3. Translocation of FtsZ in WT cells.**

603 **Movie s4. translocation of FtsZ in △*smmapZ* cells.**

604 **Movie s5. Unconstrained movement of FtsZ in △*smmapZ* cells.** The bright field image was

605 added via image calculator in Fiji.

606 **Movie s6. Unconstrained movement of FtsZ in △*smmapZ* cells.**

607 **Movie s7. Lifetime of constricting FtsZ ring in △*smmapZ* cells.**

608 **Movie s8. Lifetime of constricting FtsZ ring in WT cells.**

609 **Movie s9. Timelapse of mNeongreen_smMapZ in WT cells.**

610 **Movie s10. Single molecule tracking of smMapZ.**

611 **Movie s11. Ring structure of $Halo_{JF549}$_smMapZ.**